



Geophysical Research Letters

RESEARCH LETTER

10.1029/2018GL080635

Key Points:

- Nonlinear resonant interactions between chorus and electron cyclotron harmonic waves occurred around the magnetic equator
- Newly generated ECH sidebands exhibited frequency sweeping structures and failed to satisfy the original linear dispersion relation
- After the hot electron instabilities, the nonlinear wave-wave interactions could additionally redistribute energy among the resonant waves

Correspondence to:

Z. Su,
szpe@mail.ustc.edu.cn

Citation:

Gao, Z., Su, Z., Xiao, F., Summers, D., Liu, N., Zheng, H., et al. (2018). Nonlinear coupling between whistler-mode chorus and electron cyclotron harmonic waves in the magnetosphere. *Geophysical Research Letters*, 45, 12,685–12,693.
<https://doi.org/10.1029/2018GL080635>

Received 25 SEP 2018

Accepted 26 NOV 2018

Accepted article online 29 NOV 2018

Published online 9 DEC 2018

Nonlinear Coupling Between Whistler-Mode Chorus and Electron Cyclotron Harmonic Waves in the Magnetosphere

Zhonglei Gao^{1,2} , Zhenpeng Su^{3,4,5} , Fuliang Xiao² , Danny Summers⁶ , Nigang Liu^{3,4,5} , Huinan Zheng^{3,4,5} , Yuming Wang^{3,4,5} , Fengsi Wei¹, and Shui Wang^{3,4,5}

¹Institute of Space Science and Applied Technology, Harbin Institute of Technology, Shenzhen, China, ²School of Physics and Electronic Sciences, Changsha University of Science and Technology, Changsha, China, ³CAS Key Laboratory of Geospace Environment, Department of Geophysics and Planetary Sciences, University of Science and Technology of China, Hefei, China, ⁴Collaborative Innovation Center of Astronautical Science and Technology, University of Science and Technology of China, Hefei, China, ⁵CAS Center for Excellence in Comparative Planetology, Hefei, China, ⁶Department of Mathematics and Statistics, Memorial University of Newfoundland, St. John's, Newfoundland, Canada

Abstract Electromagnetic whistler-mode chorus and electrostatic electron cyclotron harmonic (ECH) waves can contribute significantly to auroral electron precipitation and radiation belt electron acceleration. In the past, linear and nonlinear wave-particle interactions have been proposed to explain the occurrences of these magnetospheric waves. By analyzing Van Allen Probes data, we present here the first evidence for nonlinear coupling between chorus and ECH waves. The sum-frequency and difference-frequency interactions produced the ECH sidebands with discrete frequency sweeping structures exactly corresponding to the chorus rising tones. The newly generated weak sidebands did not satisfy the original electrostatic wave dispersion relation. After the generation of chorus and normal ECH waves by hot electron instabilities, the nonlinear wave-wave interactions could additionally redistribute energy among the resonant waves, potentially affecting to some extent the magnetospheric electron dynamics.

Plain Language Summary Whistler-mode chorus and electron cyclotron harmonic emissions are two distinct magnetospheric waves responsible for auroral electron precipitation and radiation belt electron acceleration. How these magnetospheric waves are generated has remained an outstanding question. They were usually explained as a result of linear and nonlinear wave-particle interactions in early studies. By analyzing the high-resolution data of Van Allen Probes, we present here the first evidence for nonlinear coupling between chorus and electron cyclotron harmonic emissions. Such nonlinear wave-wave interactions could transfer energy among the resonant waves and affect the magnetospheric electron dynamics. This new finding will be of high interest to the communities of space plasma physics and magnetospheric physics.

1. Introduction

Whistler-mode chorus and electron cyclotron harmonic (ECH) waves are frequently observed outside the plasmapause in the magnetosphere (Helliwell, 1967; Horne et al., 1981; Kennel & Petschek, 1966; Meredith et al., 2009; Ni et al., 2011). Chorus is a right-hand polarized electromagnetic emission below the equatorial electron gyrofrequency f_{ce} and often appears as a series of discrete elements (e.g., risers, fallers, hooks, and oscillating tones) or a structureless hiss-like band in the high-resolution frequency-time spectrogram (Burtis & Helliwell, 1976; Gao et al., 2017; Santolík, Gurnett, Pickett, et al., 2003; Tsurutani & Smith, 1974). In contrast, ECH is an electrostatic emission observed as a series of harmonic bands centered around $(n+1/2)f_{ce}$ (Fredricks & Scarf, 1973; Gurnett et al., 1979; Kennel et al., 1970). Both chorus and ECH waves contribute to diffuse or pulsating auroral electron (\sim keV) precipitation (Horne et al., 2003; Lyons, 1974; Nishimura et al., 2010; Su et al., 2009, 2010; Thorne et al., 2010). Auroral electron precipitation can affect the ionospheric conductivity and the global magnetospheric convection pattern (Kan & Akasofu, 1989). Chorus waves are also able to accelerate radiation belt relativistic (\sim MeV) electrons (Horne & Thorne, 1998; Mourenas et al., 2012; Shprits et al., 2006; Su et al., 2014; Summers et al., 1998; Thorne et al., 2013), which pose a significant hazard to spaceborne systems. It is clearly important to understand the generation processes of both chorus and ECH waves.

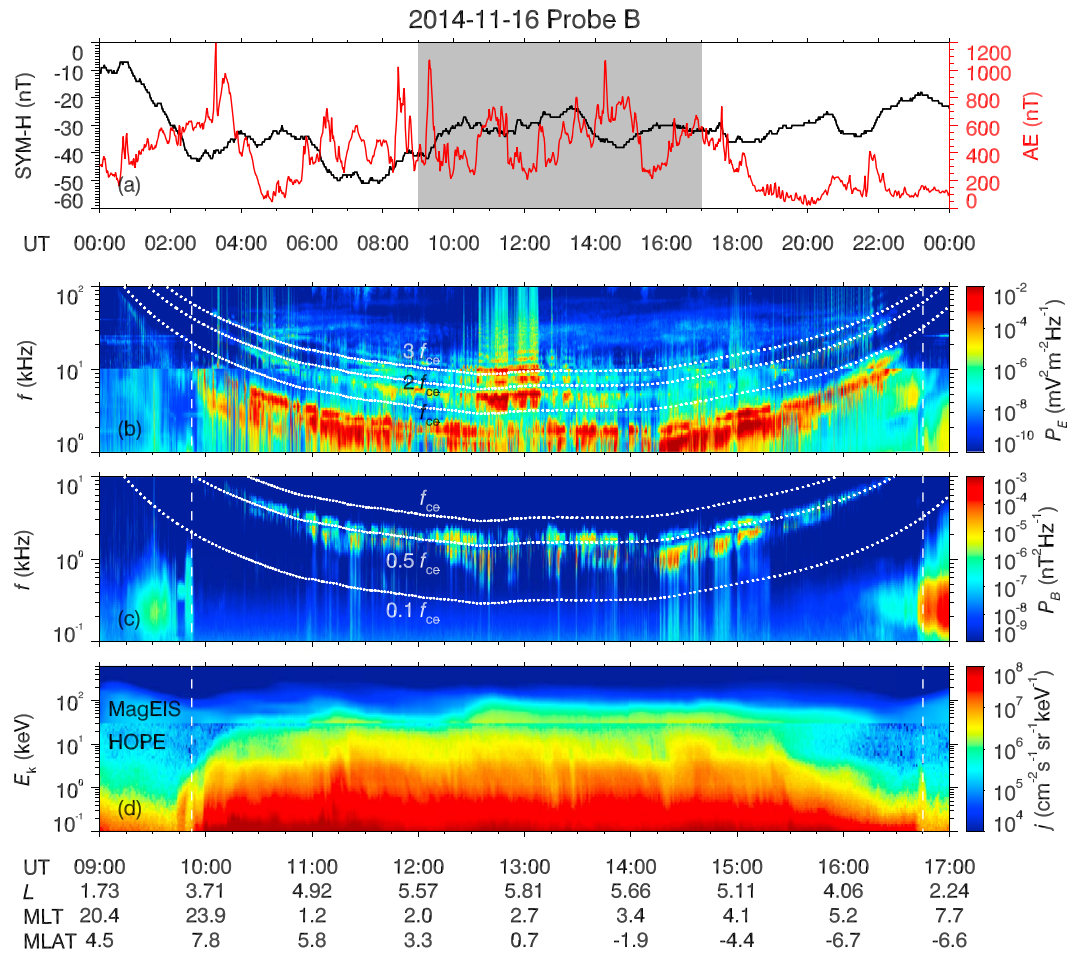


Figure 1. Space environment overview on 16 November 2014: (a) geomagnetic activity indices AE and SYM-H; (b) wave electric power spectral densities P_E ; (c) wave magnetic power spectral densities P_B ; and (d) electron differential fluxes j . In Figures 1b and 1c, the dotted lines represent $0.1f_{ce}$, $0.5f_{ce}$, f_{ce} , $2f_{ce}$, and $3f_{ce}$, respectively. In Figures 1b–1d, the vertical dashed lines mark the plasmapause locations.

Chorus and ECH waves are each thought to be excited by the loss cone instability or the temperature anisotropy instability associated with substorm-injected hot electrons (Ashour-Abdalla & Kennel, 1978; Horne et al., 2003; Li et al., 2009; Tsurutani & Smith, 1977). Linear instability theory has successfully explained the frequency distribution of chorus and ECH waves (Burtis & Helliwell, 1975; Horne & Thorne, 2000; Su et al., 2014). To account for the finer structures of chorus, such as the frequency sweeping of chorus elements and the gap between upper and lower chorus bands around $0.5f_{ce}$, various nonlinear theories have been proposed (Fu et al., 2015; Nunn et al., 1997; Omura et al., 2008; Omura & Nunn, 2011). However, the chorus and ECH instabilities are widely treated as two independent wave-particle interaction processes, although their free energies are actually provided by roughly the same electron population near the magnetic equator. In this letter, by analyzing Van Allen Probes data (Mauk et al., 2013), we present the first evidence for nonlinear coupling between chorus and ECH waves in the magnetosphere.

2. Data and Methods

The twin-satellite Van Allen Probes mission was launched on 30 August 2012, with the primary objective of understanding the fundamental physics of the Van Allen radiation belts (Mauk et al., 2013). The Electric and Magnetic Field Instrument Suite and Integrated Science (Kletzing et al., 2013) suite on this mission provides the wave power spectral densities in survey mode, the continuous-burst mode waveforms, and the background magnetic fields. Each waveform data block consists of the electromagnetic components in the nominal science payload coordinate system (with W axis along the spin axis of the satellite and U and V axes

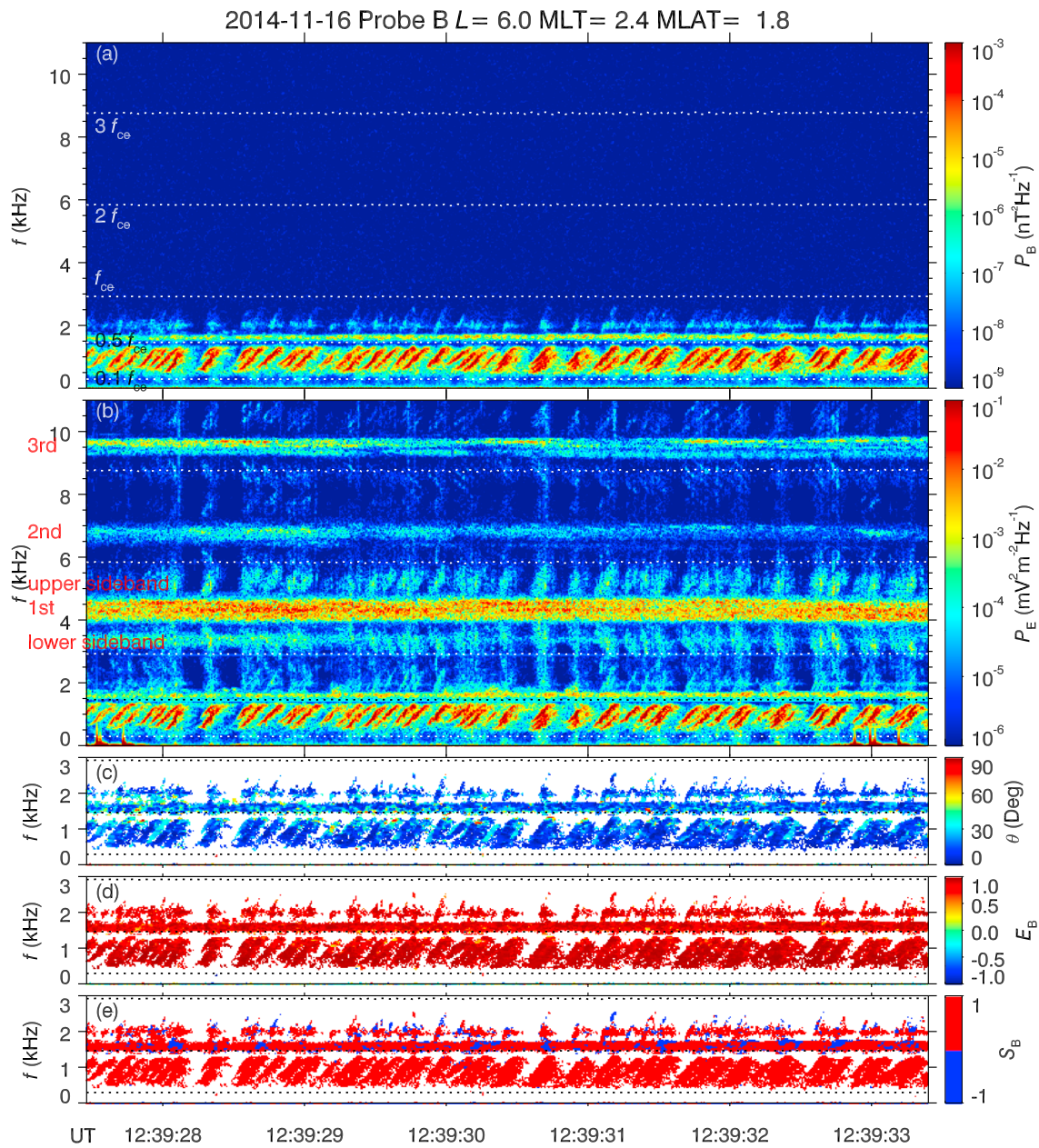


Figure 2. High-resolution power distributions and propagation and polarization characteristics of magnetosospheric waves: (a and b) electromagnetic power spectral densities P_B and P_E , (c) wave normal angles θ , (d) magnetic ellipticities E_B , and (e) signs S_B of Poynting fluxes parallel to background magnetic field. The dotted lines represent $0.1f_{ce}$, $0.5f_{ce}$, f_{ce} , $2f_{ce}$, and $3f_{ce}$.

in the spin plane) and covers a time interval of approximately 6 s with a 35-kHz sampling rate. To obtain the high-resolution wave spectral matrices, we apply a 1,024-point fast Fourier transform on these waveforms. From the cross-power spectra between electric and magnetic components, we calculate the wave Poynting fluxes (Santolík et al., 2010). Using the singular value decomposition technique (Santolík, Parrot, & Lefèuvre, 2003) on the spectral matrices, we estimate the wave normal angles and then determine the magnetic polarizations in the planes perpendicular to the wave vectors. Because of the short length of the axial electric field antenna and the strong antenna sheath impedance (Hartley et al., 2016, 2017), the electric components along the spin axis are experimentally underestimated by even up to 1 order of magnitude in the plasmatrough, and the wave electric polarization information is reliable only in the spin plane. To isolate the signals of different waves, we filter the waveforms in the frequency domain. We adopt the TS04 package (Tsyganenko & Sitnov, 2005) to model the ratios between electron gyrofrequencies at the equator and at the probe and then

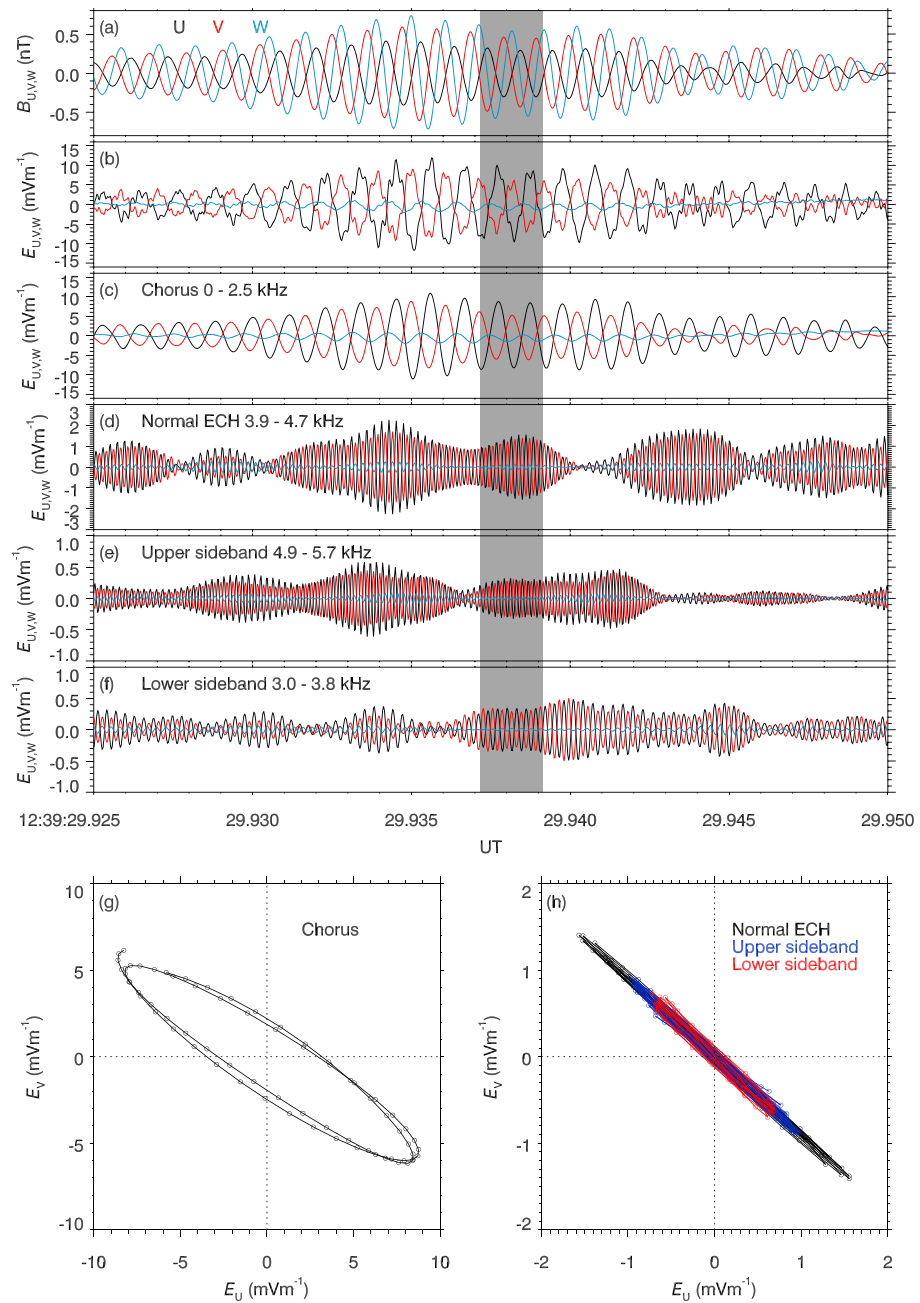


Figure 3. High-resolution waveforms and polarization characteristics of magnetospheric waves in the nominal science payload coordinate system: (a) original magnetic waveforms B_U , v , w ; (b–f) original and filtered electric waveforms E_U , v , w ; (g and h) electric polarizations of chorus, normal ECH, and newly generated sidebands in the spin plane during the time period marked by the shadow. In Figure 3h, the electric components of upper and lower sidebands have been multiplied by 3 and 2, respectively.

normalize the wave frequencies to the equatorial electron gyrofrequencies. The Helium, Oxygen, Proton, and Electron Mass Spectrometer (Funsten et al., 2013) and the Magnetic Electron Ion Spectrometer (Blake et al., 2013) of the Energetic Particle, Composition, and Thermal Plasma Suite (Spence et al., 2013) can measure the electron fluxes at energies 1.5 eV–3.8 MeV.

3. Observations

The geospace environment on 16 November 2014 is shown in Figure 1. There were a moderate storm (SYM-H minimum of -51 nT) and some strong substorms (AE maximum of 1,200 nT). Before 09:50 UT and after 16:45 UT,

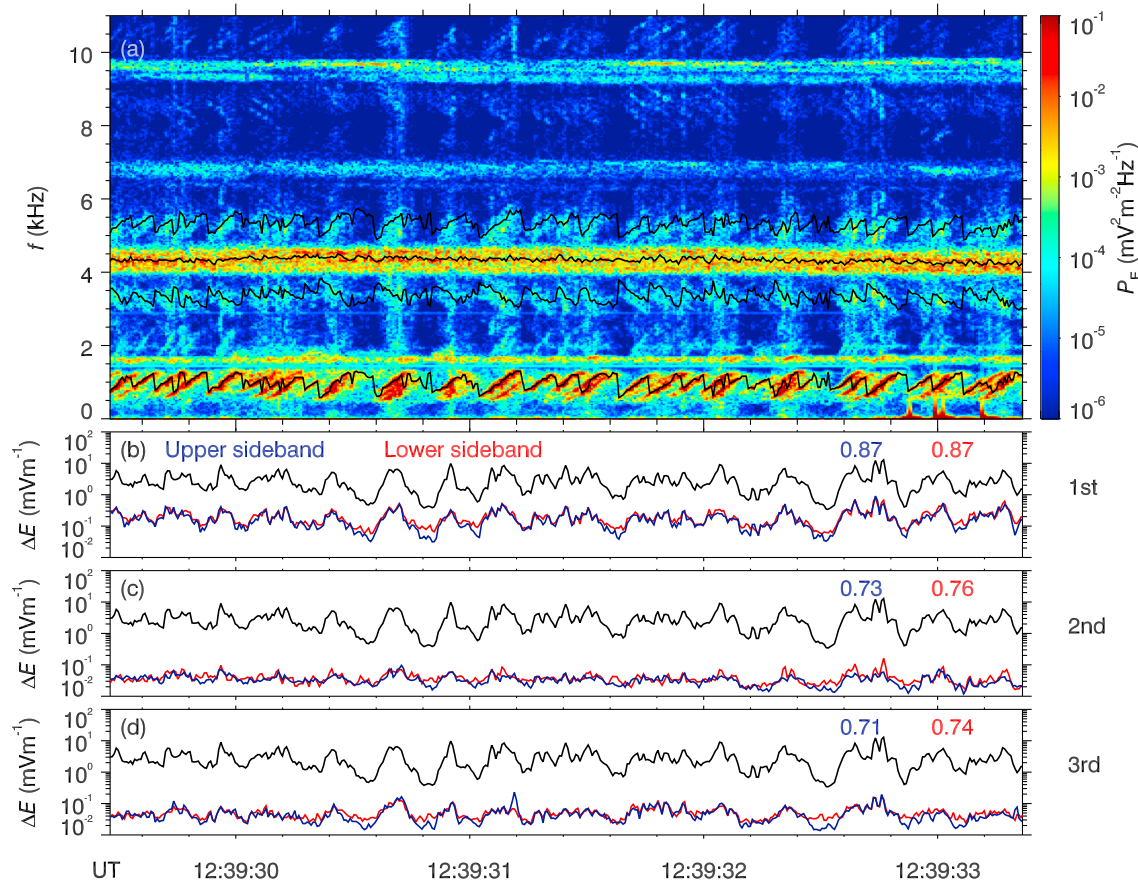


Figure 4. Correlation between chorus and ECH sidebands: (a) wave electric power spectral densities P_E with black lines for resonant wave frequencies f^C , f^E , and $f^{S\pm}$; (b–d) wave amplitudes ΔE of chorus (black) and ECH sidebands (blue for upper sideband and red for lower sideband) at three harmonics, with their correlation coefficients listed at the upper right corners.

Probe B was located in the plasmasphere and observed plasmaspheric hiss in the frequency range of 0.1–1.0 kHz. In the remained time period, corresponding to the enhancement of hot electron fluxes outside the plasmapause, Probe B detected intense chorus ($< f_{ce}$) and ECH ($> f_{ce}$) waves. The chorus emission exhibited a clear gap of wave power minimum around $0.5f_{ce}$. For the ECH emission, its first three harmonic bands were quite clear, with power peaking around the magnetic equator (12:30–13:10 UT).

Figures 2 and 3 display the high-resolution properties of magnetospheric waves around 12:39:30 UT. In the frequency-time spectrograms, the electrostatic and electromagnetic waves were obviously separated by f_{ce} . The electromagnetic chorus waves propagated quasi-parallel to the background magnetic fields with the right-hand circular magnetic polarizations in the planes perpendicular to the wave vectors. The chorus power was distributed primarily in the lower band ($< 0.5f_{ce}$) comprising successive and intense rising tones ($P_B \sim 10^{-3} nT^2 \cdot Hz^{-1}$ and $P_E \sim 10^{-1} mV^2 \cdot m^{-2} \cdot Hz^{-1}$). The electrostatic ECH emissions were composed of normal structureless harmonic bands around $(n+1/2)f_{ce}$ and unusual fishbone-like sidebands with clear rising/falling tones. In contrast to the magnetic signals with sinusoidal waveforms, the original electric signals exhibited nonsinusoidal superpositions of several frequency components. In the spin plane, the filtered electric fields of the normal ECH and its sidebands at the first harmonic were linearly polarized along the approximately same direction, essentially different from the elliptical polarization of the filtered chorus electric fields. At higher harmonics, the weak electric signals were highly polluted with noise, and their polarization information was not sufficiently clear.

Figure 4 shows the wave electric power spectrogram and the amplitudes of the lower band chorus and the ECH sidebands. The chorus peak amplitudes were about $0.01 Vm^{-1}$, 10–100 times larger than those of the ECH sidebands. There was an obvious one-to-one correlation between the discrete structures of the chorus and the ECH sidebands. At the first harmonic, the correlation coefficients between the ECH sidebands and

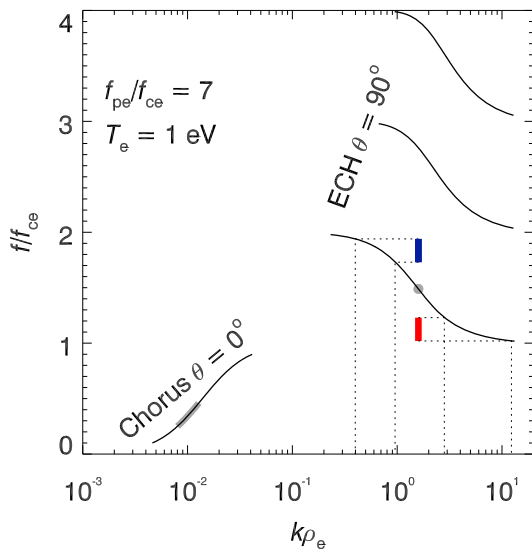


Figure 5. Dispersion relations for chorus ($\theta = 0^\circ$) and ECH ($\theta = 90^\circ$), with shadows denoting the resonant waves. The wave frequency f and the wave number k are normalized to the electron gyrofrequency f_{ce} and the gyroradius ρ_e of the cold ($T_e = 1$ eV) electrons. According to Van Allen Probes observations, the ratio of electron plasma frequency f_{pe} to electron gyrofrequency f_{ce} is set to be $f_{pe}/f_{ce} = 7$.

relations are generally consistent with those obtained from the HOTRAY code for a hot plasma (Horne, 1989; Horne & Thorne, 2000). Clearly, the wave numbers of ECH are about 2–3 orders of magnitude larger than those of chorus. The degenerated resonance condition for wave vectors $\mathbf{k}^{s\pm} = \mathbf{k}^e \pm \mathbf{k}^c \approx \mathbf{k}^e$ appears to be supported by the wave electric polarization characteristics (Figure 3h) since the electrostatic wave vectors are always parallel to the electric perturbations. For the linear electrostatic waves with frequencies $f^{s\pm}$, the normalized wave numbers $k\rho_e$ range from 0.4 to 12. The newly obtained waves with frequencies $f^{s\pm}$ but nearly constant wave numbers $k\rho_e = 1.6$ do not obey the original dispersion relation. As suggested by Hasegawa (1975), the nonlinear wave-wave interactions do not necessarily produce waves following the linear dispersion relation.

4. Discussion

Nonlinear wave-wave interaction (Craik & Adam, 1978; Franklin et al., 1975; Hruska, 1975) is a common phenomenon in the nonlinear media (e.g., radio-frequency electrical circuits, nonlinear optics, fluid mechanics, and plasma physics). Early studies had proposed the nonlinear wave-wave interaction process to explain the solar Type III radio bursts (Bardwell & Goldman, 1976; Lin et al., 1986) and the sidebands of ionospheric VLF transmitters (Park, 1981; Trakhtengerts & Hayakawa, 1993). Recently, there has been a resurgence of interest in the nonlinear wave-wave interactions within the magnetosphere. Three-wave resonances are invoked to explain the multibanded or highly oblique whistler waves (Agapitov et al., 2018; Fu et al., 2017; Gao et al., 2016; Teng et al., 2018; Vasko et al., 2018) and the magnetosonic harmonic falling/rising frequency waves (Liu et al., 2018). Here we present the first evidence for the nonlinear coupling between chorus and ECH waves and highlight the energy redistribution among the resonant waves. Initially, loss cone instability and temperature anisotropy instability of hot electrons provide the source energy of chorus and normal ECH waves. Under the condition of conservation of energy, the subsequent wave power variations ΔP should obey the Manley-Rowe relations (Manley & Rowe, 1956):

$$-\Delta P^{s+}/f^{s+} = \Delta P^e/f^e = \Delta P^c/f^c \quad (3)$$

during the sum-frequency interaction and

$$-\Delta P^{s-}/f^{s-} = \Delta P^e/f^e = -\Delta P^c/f^c \quad (4)$$

the lower band chorus reach 0.87. At the other two harmonics, probably because of the noise pollution of the weak ECH sideband signals, the obtained correlation coefficients decrease slightly to 0.71–0.76. These observations strongly imply the action of nonlinear coupling between chorus and ECH waves (e.g., Davidson, 1972; Sagdeev & Galeev, 1969).

The three-wave resonance conditions can be expressed as (e.g., Davidson, 1972; Sagdeev & Galeev, 1969)

$$f^{s\pm} = f^e \pm f^c, \quad (1)$$

$$\mathbf{k}^{s\pm} = \mathbf{k}^e \pm \mathbf{k}^c, \quad (2)$$

where f and \mathbf{k} represent the wave frequencies and wave vectors and their superscripts c , e , $s+$, and $s-$ denote chorus, ECH, and upper and lower sidebands, respectively. In Figure 4a, we examine the resonance condition for wave frequencies at the first harmonic where the intense sideband signals are conducive to the identification of the frequency-sweeping structures. At every time point, f^e is specified as the power-weighted center frequency for the normal structureless ECH band, and f^c is determined as the peak power frequency for the lower band chorus. The obtained frequencies $f^{s\pm} = f^e \pm f^c$ are found to well characterize the frequency profiles of the ECH sidebands. Unfortunately, the single point observations do not allow the calculation of wave vectors. In Figure 5, we plot the linear dispersion relations for the parallel-propagating chorus (Stix, 1992) and the perpendicular-propagating ECH waves (Davidson, 1972). Such dispersion

during the difference-frequency interaction. Substituting (1) into (3) and (4), we can easily verify the conservation of energy $\Delta P^{s\pm} + \Delta P^e + \Delta P^c = 0$. From (3) and (4), we find the net changes in the chorus and ECH wave power are given, respectively, by

$$\Delta P^c = f^c(\Delta P^{s-}/f^{s-} - \Delta P^{s+}/f^{s+}), \quad (5)$$

$$\Delta P^e = -f^e(\Delta P^{s+}/f^{s+} + \Delta P^{s-}/f^{s-}). \quad (6)$$

Under the condition of $\Delta P^{s-} = \Delta P^{s+} > 0$ (Figure 4), equations (5) and (6) imply a net energy transfer from the normal ECH bands to the discrete structures of the ECH sidebands and the lower band chorus. Even slightly enhanced chorus waves are favorable for auroral electron precipitation and radiation belt electron acceleration. According to the Doppler-shifted N th-order resonance condition, the electron resonant parallel velocity can be expressed as (e.g., Horne & Thorne, 2000)

$$v_{\parallel} = \frac{2\pi(f - Nf_{ce})}{k_{\parallel}}. \quad (7)$$

Note that both normal ECH and its sidebands probably have a small parallel wave number k_{\parallel} (Ashour-Abdalla & Kennel, 1978). Compared to the normal ECH, the ECH sidebands have frequencies closer to the electron gyrofrequency harmonics and likely interact with electrons at lower energies. However, because the transferred energy among the resonant waves appears to be only a small proportion of the initial energy of chorus and normal ECH waves from the hot electron instabilities (Figure 4), these additional effects of the nonlinear wave-wave interactions on the magnetospheric electrons may be limited.

5. Summary

Chorus and ECH are two important magnetospheric wave modes (e.g., Artemyev et al., 2013; Kasahara et al., 2018; Ni et al., 2017; Reeves et al., 2013; Thorne et al., 2013, 2010). Different from the normal structureless ECH bands, upper and lower sidebands of ECH consisting of discrete frequency-sweeping structures were observed to occur near the magnetic equator. These discrete structures of ECH sidebands exhibited a clear one-to-one correlation with the rising tones of lower band chorus. Quantitatively, the correlation coefficients between the electric amplitudes of lower band chorus and ECH sidebands were 0.71–0.87. For the first time, these observations demonstrate nonlinear coupling between chorus and ECH waves in the magnetosphere. The sum-frequency and difference-frequency interactions produced the upper and lower sidebands of ECH, respectively. These newly generated weak sidebands did not satisfy the original dispersion relation for electrostatic waves. After the generation of chorus and normal ECH waves by the loss cone instability and the temperature anisotropy instability associated with substorm-injected hot electrons, the nonlinear wave-wave interactions could additionally redistribute energy among the resonant waves, thereby potentially affecting to some extent the magnetospheric electron dynamics.

Acknowledgments

We acknowledge Van Allen

Probes teams for the use of data.
Data are available at the websites
<http://emfisis.physics.uiowa.edu/Flight/> for EMFISIS and http://www.rbsp-ect.lanl.gov/data_pub/ for ECT. This work was supported by the National Natural Science Foundation of China Grants 41631071, 41804171, and 41774170; the Chinese Academy of Sciences Grants KZCX2-EW-QN510 and KZZD-EW-01-4; the CAS Key Research Program of Frontier Sciences Grant QYZDB-SSW-DQC015; and the National Key Basic Research Special Foundation of China Grant 2011CB811403. D. S. acknowledges support from a Discovery Grant of the Natural Sciences and Engineering Research Council of Canada.

References

- Agapitov, O., Drake, J. F., Vasko, I., Mozer, F. S., Artemyev, A., Krasnoselskikh, V., & Reeves, G. D. (2018). Nonlinear electrostatic steepening of whistler waves: The guiding factors and dynamics in inhomogeneous systems. *Geophysical Research Letter*, 45(5), 2168–2176. <https://doi.org/10.1002/2017GL076957>
- Artemyev, A. V., Agapitov, O. V., Mourenas, D., Krasnoselskikh, V., & Zelenyi, L. M. (2013). Storm-induced energization of radiation belt electrons: Effect of wave obliquity. *Geophysical Research Letters*, 40, 4138–4143. <https://doi.org/10.1002/grl.50837>
- Ashour-Abdalla, M., & Kennel, C. F. (1978). Nonconvective and convective electron cyclotron harmonic instabilities. *Journal of Geophysical Research*, 83, 1531–1543. <https://doi.org/10.1029/JA083IA04p01531>
- Bardwell, S., & Goldman, M. V. (1976). Three-dimensional Langmuir wave instabilities in type III solar radio bursts. *Astrophysical Journal*, 209, 912–926. <https://doi.org/10.1086/154790>
- Blake, J. B., Carranza, P. A., Claudepierre, S. G., Clemons, J. H., Crain, W. R., Dotan, Y., & Zakrzewski, M. P. (2013). The magnetic electron ion spectrometer (MagEIS) instruments aboard the Radiation Belt Storm Probes (RBSP) Spacecraft. *Space Science Reviews*, 179, 383–421. <https://doi.org/10.1007/s11214-013-9991-8>
- Burtis, W. J., & Helliwell, R. A. (1975). Magnetospheric chorus—Amplitude and growth rate. *Journal of Geophysical Research*, 80, 3265–3270. <https://doi.org/10.1029/JA080i022p03265>
- Burtis, W. J., & Helliwell, R. A. (1976). Magnetospheric chorus—Occurrence patterns and normalized frequency. *Planetary and Space Science*, 24, 1007–1024. [https://doi.org/10.1016/0032-0633\(76\)90119-7](https://doi.org/10.1016/0032-0633(76)90119-7)
- Craig, A., & Adam, J. (1978). Evolution in space and time of resonant wave triads. I. The ‘pump-wave approximation’. *Proceedings of the Royal Society*, 363(1713), 243–255. <https://doi.org/10.1098/rspa.1978.0166>
- Davidson, R. C. (1972). *Methods in nonlinear plasma theory*. New York: Academic Press.

- Franklin, R., Hamberger, S., Lampis, G., & Smith, G. (1975). Nonlinear behaviour of a finite amplitude electron plasma wave I. Electron trapping effects. *Proceedings of the Royal Society of London A*, 347(1648), 1–24. <https://doi.org/10.1098/rspa.1975.0194>
- Fredricks, R. W., & Scarf, F. L. (1973). Recent studies of magnetospheric electric field emissions above the electron gyrofrequency. *Journal of Geophysical Research*, 78, 310–314. <https://doi.org/10.1029/JA078i001p00310>
- Fu, X., Gary, S. P., Reeves, G. D., Winske, D., & Woodroffe, J. R. (2017). Generation of highly oblique lower band chorus via nonlinear three-wave resonance. *Geophysical Research Letters*, 44, 9532–9538. <https://doi.org/10.1002/2017GL074411>
- Fu, X., Guo, Z., Dong, C., & Gary, S. P. (2015). Nonlinear sub-cyclotron resonance as a formation mechanism for gaps in banded chorus. *Geophysical Research Letters*, 42, 3150–3159. <https://doi.org/10.1002/2015GL064182>
- Funsten, H. O., Skoug, R. M., Guthrie, A. A., MacDonald, E. A., Baldonado, J. R., Harper, R. W., & Chen, J. (2013). Helium, oxygen, proton, and electron (HOPE) mass spectrometer for the Radiation Belt Storm Probes Mission. *Space Science Reviews*, 179, 423–484. <https://doi.org/10.1007/s11214-013-9968-7>
- Gao, X., Lu, Q., Bortnik, J., Li, W., Chen, L., & Wang, S. (2016). Generation of multiband chorus by lower band cascade in the Earth's magnetosphere. *Geophysical Research Letters*, 43, 2343–2350. <https://doi.org/10.1002/2016GL068313>
- Gao, Z., Su, Z., Chen, L., Zheng, H., Wang, Y., & Wang, S. (2017). Van Allen Probes observations of whistler-mode chorus with long-lived oscillating tones. *Geophysical Research Letters*, 44, 5909–5919. <https://doi.org/10.1002/2017GL073420>
- Gurnett, D. A., Anderson, R. R., Tsurutani, B. T., Smith, E. J., Paschmann, G., Haerendel, G., & Russell, C. T. (1979). Plasma wave turbulence at the magnetopause—Observations from ISEE 1 and 2. *Journal of Geophysical Research*, 84, 7043–7058. <https://doi.org/10.1029/JA084iA12p07043>
- Hartley, D. P., Kletzing, C. A., Kurth, W. S., Bounds, S. R., Averkamp, T. F., Hospodarsky, G. B., & Watt, C. E. J. (2016). Using the cold plasma dispersion relation and whistler mode waves to quantify the antenna sheath impedance of the Van Allen Probes EFW instrument. *Journal of Geophysical Research: Space Physics*, 121, 4590–4606. <https://doi.org/10.1002/2016JA022501>
- Hartley, D. P., Kletzing, C. A., Kurth, W. S., Hospodarsky, G. B., Bounds, S. R., Averkamp, T. F., & Wygant, J. R. (2017). An improved sheath impedance model for the Van Allen Probes EFW instrument: Effects of the spin axis antenna. *Journal of Geophysical Research: Space Physics*, 122, 4420–4429. <https://doi.org/10.1002/2016ja023597>
- Hasegawa, A. (1975). *Plasma instabilities and nonlinear effects*. Berlin: Springer.
- Helliwell, R. A. (1967). A theory of discrete VLF emissions from the magnetosphere. *Journal of Geophysical Research*, 72, 4773–4790. <https://doi.org/10.1029/JZ072i019p04773>
- Horne, R. B. (1989). Path-integrated growth of electrostatic waves: The generation of terrestrial myriametric radiation. *Journal of Geophysical Research*, 94(A7), 8895. <https://doi.org/10.1029/JA094iA07p08895>
- Horne, R. B., Christiansen, P. J., Gough, M. P., Ronnmark, K. G., Johnson, J. F. E., Sojka, J., & Wrenn, G. L. (1981). Amplitude variations of electron cyclotron harmonic waves. *Nature*, 294, 338–340. <https://doi.org/10.1038/294338a0>
- Horne, R. B., & Thorne, R. M. (1998). Potential waves for relativistic electron scattering and stochastic acceleration during magnetic storms. *Geophysical Research Letters*, 25, 3011–3014. <https://doi.org/10.1029/98GL01002>
- Horne, R. B., & Thorne, R. M. (2000). Electron pitch angle diffusion by electrostatic electron cyclotron harmonic waves: The origin of pancake distributions. *Journal of Geophysical Research*, 105, 5391–5402. <https://doi.org/10.1029/1999JA00447>
- Horne, R. B., Thorne, R. M., Meredith, N. P., & Anderson, R. R. (2003). Diffuse auroral electron scattering by electron cyclotron harmonic and whistler mode waves during an isolated substorm. *Journal of Geophysical Research*, 108, 1290. <https://doi.org/10.1029/2002JA009736>
- Hruska, A. (1975). Interactions between electrostatic and electromagnetic waves in a magnetized plasma. *Plasma Physics*, 17(12), 1165. <https://doi.org/10.1088/0032-1028/17/12/016>
- Kan, J. R., & Akasofu, S. I. (1989). Electrodynamics of solar wind-magnetosphere-ionosphere interactions. *IEEE Transactions on Plasma Science*, 17, 83–108. <https://doi.org/10.1109/27.24612>
- Kasahara, S., Miyoshi, Y., Yokota, S., Mitani, T., Kasahara, Y., Matsuda, S., & Shinohara, I. (2018). Pulsating aurora from electron scattering by chorus waves. *Nature*, 554, 337–340. <https://doi.org/10.1038/nature25505>
- Kennel, C. F., & Petschek, H. E. (1966). Limit on stably trapped particle fluxes. *Journal of Geophysical Research*, 71, 1–28. <https://doi.org/10.1029/JZ071i001p00001>
- Kennel, C. F., Scarf, F. L., Fredricks, R. W., McGehee, J. H., & Coroniti, F. V. (1970). VLF electric field observations in the magnetosphere. *Journal of Geophysical Research*, 75, 6136–6152. <https://doi.org/10.1029/JA075i031p06136>
- Kletzing, C. A., Kurth, W. S., Acuna, M., MacDowall, R. J., Torbert, R. B., Averkamp, T., & Tyler, J. (2013). The electric and magnetic field instrument suite and integrated science (EMFISIS) on RBSP. *Space Science Reviews*, 179, 127–181. <https://doi.org/10.1007/s11214-013-9993-6>
- Li, W., Thorne, R. M., Angelopoulos, V., Bonnell, J. W., McFadden, J. P., Carlson, C. W., & Auster, H. U. (2009). Evaluation of whistler-mode chorus intensification on the nightside during an injection event observed on the THEMIS spacecraft. *Journal of Geophysical Research*, 114, A00C14. <https://doi.org/10.1029/2008JA013554>
- Lin, R. P., Levedahl, W. K., Lotko, W., Gurnett, D. A., & Scarf, F. L. (1986). Evidence for nonlinear wave-wave interactions in solar type III radio bursts. *Astrophysical Journal*, 308, 954–965. <https://doi.org/10.1086/164563>
- Liu, N., Su, Z., Zheng, H., Wang, Y., & Wang, S. (2018). Magnetosonic harmonic falling and rising frequency emissions potentially generated by nonlinear wave-wave interactions in the Van Allen radiation belts. *Geophysical Research Letters*, 45, 7985–7995. <https://doi.org/10.1029/2018GL079232>
- Lyons, L. R. (1974). Electron diffusion driven by magnetospheric electrostatic waves. *Journal of Geophysical Research*, 79, 575–580. <https://doi.org/10.1029/JA079i004p00575>
- Manley, J. M., & Rowe, H. E. (1956). Part I part i. *Proceedings of the IRE*, 44(7), 904–913. <https://doi.org/10.1109/JRPROC.1956.275145>
- Mauk, B. H., Fox, N. J., Kanekal, S. G., Kessel, R. L., Sibeck, D. G., & Ukhorskiy, A. (2013). Science objectives and rationale for the Radiation Belt Storm Probes Mission. *Space Science Reviews*, 179, 3–27. <https://doi.org/10.1007/s11214-012-9908-y>
- Meredith, N. P., Horne, R. B., Thorne, R. M., & Anderson, R. R. (2009). Survey of upper band chorus and ECH waves: Implications for the diffuse aurora. *Journal of Geophysical Research*, 114, A07218. <https://doi.org/10.1029/2009ja014230>
- Mourenas, D., Artemyev, A., Agapitov, O., & Krasnoselskikh, V. (2012). Acceleration of radiation belt electrons by oblique chorus waves. *Journal Geophysical Research*, 117, A10212. <https://doi.org/10.1029/2012ja018041>
- Ni, B., Gu, X., Fu, S., Xiang, Z., & Lou, Y. (2017). A statistical survey of electrostatic electron cyclotron harmonic waves based on THEMIS FFF wave data. *Journal of Geophysical Research: Space Physics*, 122, 3342–3353. <https://doi.org/10.1002/2016JA023433>
- Ni, B., Thorne, R., Liang, J., Angelopoulos, V., Cully, C., Li, W., & Roux, A. (2011). Global distribution of electrostatic electron cyclotron harmonic waves observed on THEMIS. *Geophysical Research Letters*, 38, L17105. <https://doi.org/10.1029/2011GL048793>
- Nishimura, Y., Bortnik, J., Li, W., Thorne, R. M., Lyons, L. R., Angelopoulos, V., & Auster, U. (2010). Identifying the driver of pulsating aurora. *Science*, 330, 81. <https://doi.org/10.1126/science.1193186>

- Nunn, D., Omura, Y., Matsumoto, H., Nagano, I., & Yagitani, S. (1997). The numerical simulation of VLF chorus and discrete emissions observed on the Geotail satellite using a Vlasov code. *Journal of Geophysical Research*, 102, 27,083–27,098. <https://doi.org/10.1029/97JA02518>
- Omura, Y., Kato, Y., & Summers, D. (2008). Theory and simulation of the generation of whistler-mode chorus. *Journal of Geophysical Research*, 113, 4223. <https://doi.org/10.1029/2007JA012622>
- Omura, Y., & Nunn, D. (2011). Triggering process of whistler mode chorus emissions in the magnetosphere. *Journal of Geophysical Research*, 116(5), 1–10. <https://doi.org/10.1029/2010JA016280>
- Park, C. (1981). Generation of whistler-mode sidebands in the magnetosphere. *Journal of Geophysical Research*, 86(A4), 2286–2294. <https://doi.org/10.1029/JA086iA04p02286>
- Reeves, G. D., Spence, H. E., Henderson, M. G., Morley, S. K., Friedel, R. H. W., Funsten, H. O., et al. (2013). Electron acceleration in the heart of the Van Allen radiation belts. *Science*, 341(6149), 991–994.
- Sagdeev, R. Z., & Galeev, A. A. (1969). *Nonlinear plasma theory*. New York: W. A. Benjamin, Inc.
- Santolík, O., Gurnett, D. A., Pickett, J. S., Parrot, M., & Cornilleau-Wehrlin, N. (2003). Spatio-temporal structure of storm-time chorus. *Journal of Geophysical Research*, 108, 1278. <https://doi.org/10.1029/2002JA009791>
- Santolík, O., Parrot, M., & Lefèuvre, F. (2003). Singular value decomposition methods for wave propagation analysis. *Radio Science*, 38(1), 1010. <https://doi.org/10.1029/2000RS002523>
- Santolík, O., Pickett, J. S., Gurnett, D. A., Menietti, J. D., Tsurutani, B. T., & Verkhoglyadova, O. (2010). Survey of Poynting flux of whistler mode chorus in the outer zone. *Journal of Geophysical Research*, 115, 1–13. <https://doi.org/10.1029/2009JA014925>
- Shprits, Y. Y., Thorne, R. M., Horne, R. B., Glauert, S. A., Cartwright, M., Russell, C. T., & Kanekal, S. G. (2006). Acceleration mechanism responsible for the formation of the new radiation belt during the 2003 halloween solar storm. *Geophysical Research Letters*, 33, L05104. <https://doi.org/10.1029/2005GL024256>
- Spence, H. E., Reeves, G. D., Baker, D. N., Blake, J. B., Bolton, M., Bourdarie, S., & Thorne, R. M. (2013). Science goals and overview of the energetic particle, composition, and thermal plasma (ECT) suite on NASAs Radiation Belt Storm Probes (RBSP) Mission. *Space Science Reviews*, 179, 311–336. <https://doi.org/10.1007/s11214-013-0007-5>
- Stix, T. H. (1992). *Waves in Plasmas*. New York: American Institute of Physics.
- Su, Z., Xiao, F., Zheng, H., He, Z., Zhu, H., Zhang, M., & Baker, D. N. (2014). Nonstorm time dynamics of electron radiation belts observed by the Van Allen Probes. *Geophysical Research Letters*, 41, 229–235. <https://doi.org/10.1002/2013GL058912>
- Su, Z., Zheng, H., & Wang, S. (2009). Evolution of electron pitch angle distribution due to interactions with whistler mode chorus following substorm injections. *Journal of Geophysical Research*, 114, A08202. <https://doi.org/10.1029/2009JA014269>
- Su, Z., Zheng, H., & Wang, S. (2010). A parametric study on the diffuse auroral precipitation by resonant interaction with whistler-mode chorus. *Journal of Geophysical Research*, 115, A05219. <https://doi.org/10.1029/2009JA014759>
- Su, Z., Zhu, H., Xiao, F., Zheng, H., Wang, Y., He, Z., & Wygant, J. R. (2014). Intense duskside lower band chorus waves observed by Van Allen Probes: Generation and potential acceleration effect on radiation belt electrons. *Journal of Geophysical Research: Space Physics*, 119, 4266–4273. <https://doi.org/10.1002/2014JA019919>
- Summers, D., Thorne, R. M., & Xiao, F. (1998). Relativistic theory of wave-particle resonant diffusion with application to electron acceleration in the magnetosphere. *Journal of Geophysical Research*, 103, 20487. <https://doi.org/10.1029/98JA01740>
- Teng, S., Zhao, J., Tao, X., Wang, S., & Reeves, G. (2018). Observation of oblique lower band chorus generated by nonlinear three-wave interaction. *Geophysical Research Letters*, 45, 6343–6352. <https://doi.org/10.1029/2018GL078765>
- Thorne, R. M., Li, W., Ni, B., Ma, Q., Bortnik, J., Chen, L., & Kanekal, S. G. (2013). Rapid local acceleration of relativistic radiation-belt electrons by magnetospheric chorus. *Nature*, 504, 411–414. <https://doi.org/10.1038/nature12889>
- Thorne, R. M., Ni, B., Tao, X., Horne, R. B., & Meredith, N. P. (2010). Scattering by chorus waves as the dominant cause of diffuse auroral precipitation. *Nature*, 467, 943. <https://doi.org/10.1038/nature09467>
- Trakhtengerts, V. Y., & Hayakawa, M. (1993). A wave-wave interaction in whistler frequency range in space plasma. *Journal of Geophysical Research*, 98(A11), 19,205–19,217. <https://doi.org/10.1029/93JA01640>
- Tsurutani, B. T., & Smith, E. J. (1974). Postmidnight chorus: A substorm phenomenon. *Journal of Geophysical Research*, 79(1), 118–127. <https://doi.org/10.1029/JA079i001p00118>
- Tsurutani, B. T., & Smith, E. J. (1977). Two types of magnetospheric ELF chorus and their substorm dependences. *Journal of Geophysical Research*, 82, 5112–5128. <https://doi.org/10.1029/JA082i032p05112>
- Tsyganenko, N. A., & Sitnov, M. I. (2005). Modeling the dynamics of the inner magnetosphere during strong geomagnetic storms. *Journal of Geophysical Research*, 110, A03208. <https://doi.org/10.1029/2004JA010798>
- Vasko, I. Y., Agapitov, O. V., Mozer, F. S., Bonnell, J. W., Artemyev, A. V., Krasnoselskikh, V. V., & Tong, Y. (2018). Electrostatic steepening of whistler waves. *Physical Review Letters*, 120(19), 195101. <https://doi.org/10.1103/PhysRevLett.120.195101>